Post-print version:

Coordinated Frequency Control Using MT-HVDC Grids With Wind Power Plants

Fernando D. Bianchi and José Luis Domínguez-García

BibTeX:

Coordinated frequency control using MT-HVDC grids with wind power plants

Fernando D. Bianchi and José Luis Domínguez-García *Member, IEEE*

Abstract—In the last years, wind power has continuously increased the participation in the power generation share. For transmitting the power generated from wind power plants (WPPs) to AC grids, multi–terminal HVDC systems are envisaged as the future backbone of a European SuperGrid interconnecting wind power generation with various AC grids and countries. The article presents a coordinated control scheme in order that offshore WPPs connected through multi–terminal HVDC systems are able to contribute to the primary frequency control of the land AC grids. The proposed control scheme is capable of achieving a suitable frequency regulation even under low wind power conditions by allowing also the power share among AC areas. The control scheme is evaluated by dynamic simulations in an adapted version of the Cigré DC grid benchmark with a 5-terminal HVDC grid including two wind farms and three AC networks.

Index Terms—Distributed control, primary frequency support, grid integration, multi–terminal HVDC grids, wind power plants

I. INTRODUCTION

WIND power expansion and the increase on both size and power ratings of wind farms are fostering their installation in offshore locations, where winds are less variable and there are fewer space restrictions [1]. The current trend is also towards locating these offshore wind power plants (WPPs) far from shore (above 60 km). For such long distances, the use of High Voltage Direct Current (HVDC) technologies for the power transmission are more cost-effective than conventional High Voltage Alternating Current (HVAC) (for distances between 60 and 90 km as break-even point). Moreover, the increase in the number of offshore wind farms has allowed envisaging the use of these installations for power sharing between systems in different countries. An example of this concept is the so-called European SuperGrid [2]. Multi-terminal HVDC networks (MT-HVDC) may be used to create this Pan-European transmission grid aimed at reducing power losses and reactive compensation in the power distribution [3], [4]. Another advantage of HVDC technologies is their high capability to regulate the power flowing through the terminals.

A side-effect of the expansion of wind power generation and HVDC technologies is the reduction of power system global

inertia, which is modifying power system dynamic response. This fact has forced Transmission System Operators (TSOs) to develop new grid requirements for both renewable sources and HVDC based systems in order to ensure stable and secure operation of power systems [5]–[7]. Among others, these new codes establish that WPPs and HVDC systems should contribute to the frequency stability by regulating the injected active power [8]. Frequency stability requires to maintain a power balance as any generation-consumption mismatch may cause drifts of the AC network frequency [9]. Since WPPs and MT-HVDC systems are capable of achieving faster active power regulation than the conventional generators, they are expected to contribute to primary frequency control, *i.e.*, to the first control protection against frequency instability [10].

In general, WPPs can provide frequency support mainly in two different ways depending on the desired contribution to be provided. By delivering the kinetic energy naturally stored in the wind turbines for inertial response and by maintaining certain power reserves when focusing on slow primary frequency response. These have been extensively studied in the literature, see for example [11]–[14]. The power reserve is obtained by operating the wind turbines at a non-optimal point by pitching or over-speeding. In the case of MT-HVDC systems, the frequency control strategies aimed at ensuring power balance by sharing power reserves among the AC grids connected to the DC grid [15]–[18]. These strategies use distributed control concepts such as consensus algorithms. Only few research studies can be found about the use of WPPs connected through MT-HVDC grids to provide frequency support. Bucurenciu [19] uses WPPs for frequency control, but do not fully exploit the MT-HVDC system capabilities for power sharing. In [20], a communication-less scheme is proposed using droop and dead-band control to provide inertial and primary frequency control. In [21], the fiber optic link available in the DC cables is used to emulate the frequency variations on the AC areas in the wind power stations and thus providing inertial response. In these two articles, the power reserve limits are not explicitly considered in the proposed control schemes, nor the stability analysis of the entire system.

This article deals with the primary frequency control using not only offshore WPPs connected to mainland through MT-HVDC networks but also, if needed, the other AC grids connected to the MT-HVDC transmission system. The proposed strategy coordinates the power injected and extracted from the MT-HVDC by the onshore and offshore stations considering explicitly the limited reserves available in the WPPs. The control scheme consists of a distributed PI control scheme plus a consensus algorithm (similar to those presented in [15],
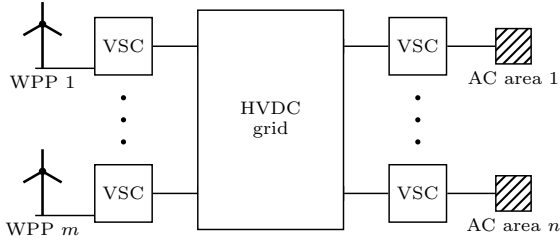
Figure 1. Multi-terminal HVDC network connecting AC areas and WPPs

[16]). The WPPs are used as active power sources in order to compensate imbalances in the AC areas and thus maintaining the frequency close to the nominal values. When there is sufficient power reserve in the WPPs, the proposed control scheme is capable of restoring the frequency to the nominal values. In case of large power imbalances, the algorithm seeks to minimize the frequency deviations by sharing the power reserves in WPPs and AC areas. A design procedure to ensure stability of the entire system and the computation of the final frequencies after a power disturbance is provided. The control scheme is evaluated by dynamic simulations in a 5-terminal HVDC network based on the Cigré DC grid adapted for frequency stability studies under representative scenarios, including communications faults.

II. MT-HVDC NETWORKS CONNECTING WPPS

Fig. 1 sketches a typical MT-HVDC network connecting n AC areas with m WPPs. Both the AC areas and WPPs are connected to the DC grid through Voltage Source Converters (VSCs). The goal is to transfer the wind power through the HVDC grid towards the AC areas where the consumers are located. Although the main purpose of the system is the transmission of the power generated by the wind farms, as previously mentioned, the system can also provide frequency support for the AC areas. To this end, WPPs must keep a certain power reserve in order to compensate the temporary power imbalances in the AC areas by taking advantage of the capability of WPPs for providing fast active power contribution.

In frequency stability analysis, the AC conventional generation based grids can be represented as a power balance (generation and load) with dynamics dominated by slow synchronous conventional generators. Therefore, each AC area is modelled as a single aggregated synchronous generator and a frequency dependent load [22]. Thus, the dynamics of the i-th AC area ($i = 1, \ldots, n$) can be represented by

$$J_i \frac{df_i}{dt} = \frac{P_{m,i} - P_{l,i} - P_{dc,i}}{4\pi^2 f_i} - D_{g,i}(f_i - f_{\text{nom},i}), \quad (1)$$

$$\tau_{m,i} \frac{dP_{m,i}}{dt} = \bar{P}_{m,i} - P_{m,i} - \frac{P_{\text{nom},i}}{\sigma_i f_{\text{nom},i}}(f_i - f_{\text{nom},i}), \quad (2)$$

where f_i is the electrical frequency, $f_{\text{nom},i}$ the nominal frequency, σ_i, J_i and $D_{g,i}$ are the droop, the inertia and the damping of the generator, respectively, $P_{m,i}$ the mechanical power, $P_{l,i}$ the power demand on the area, and $P_{dc,i}$ is the DC power extracted from the multi-terminal network. The synchronous generator has a speed governor with a time constant

$\tau_{m,i}$ and reference $\bar{P}_{m,i}$. This reference is assumed imposed by a secondary frequency control in periods within 30 s. Such reference can be assumed constant since its dynamics are slower than the primary frequency control response. The aggregated load in the AC area is represented as

$$P_{l,i} = \bar{P}_{l,i}(1 + D_{l,i}(f_i - f_{\text{nom},i})),$$

where $D_{l,i}$ is the load damping and $\bar{P}_{l,i}$ the power demand at equilibrium.

Defining the following variables

$$\begin{aligned} y_i &= f_i - f_{\text{nom},i}, & x_i &= P_{m,i} - \bar{P}_{m,i}, \\ u_i &= P_{dc,i} - \bar{P}_{dc,i}, & d_i &= P_{l,i} - \bar{P}_{l,i}, \end{aligned}$$

and linearizing (1), the local dynamics of the i-th AC area is governed by

$$\frac{dy_i}{dt} = -a_{1,i}y_i + a_{2,i}(x_i - d_i - u_i), \quad (3)$$

$$\frac{dx_i}{dt} = -a_{3,i}y_i - a_{4,i}x_i, \quad (4)$$

where $\bar{P}_{dc,i}$ is the power extracted from the MT-HVDC grid at equilibrium and

$$a_{1,i} = \frac{D_{g,i} + \bar{P}_{l,i}D_{l,i}/(4\pi^2 f_{\text{nom},i})}{J_i}, \quad a_{2,i} = \frac{1}{4\pi^2 f_{\text{nom},i}J_i},$$

$$a_{3,i} = \frac{P_{\text{nom},i}}{\tau_{m,i}\sigma_i f_{\text{nom},i}}, \quad a_{4,i} = \frac{1}{\tau_{m,i}}.$$

For control design purpose, the dynamics of the WPPs can be neglected. In frequency support the expected time constants are in the range of seconds, which is much slower than the response times of the power converters interfacing the WPPs. Therefore, they are considered as power sources delivering into the DC grid a power $P_{w,i}$ ($i = 1, \ldots, m$). WPP control schemes for this purpose can be found for example in [23]. It is worth noticing that fast active power contributions can provoke undesirable stresses in the mechanical structures of the wind turbines. This can be considered during the control design by imposing constraints on the control signals.

Taking into account that the phenomena associated with frequency changes in power systems are slow, the DC grid can be represented as a resistive electrical network, neglecting existing inductances and capacitances of the cables, which present faster dynamics. Therefore, the power injected or extracted from the DC grid by the i-th station is given by

$$V_{dc,i} \frac{V_{dc,i} - V_{dc,j}}{R_{ij}},$$

where R_{ij} is the resistance between nodes i and j and $V_{dc,i}$ the DC voltage at the node i.

III. COORDINATED CONTROL SCHEME FOR FREQUENCY SUPPORT

In this section, a coordinated control scheme is proposed in order that WPPs are able to contribute to the frequency support provision in the synchronous AC areas. The proposed control is distributed, i.e. without a main supervisor, in order to take into account the fact that the multi-terminal stations can be operated by different TSOs or system players.
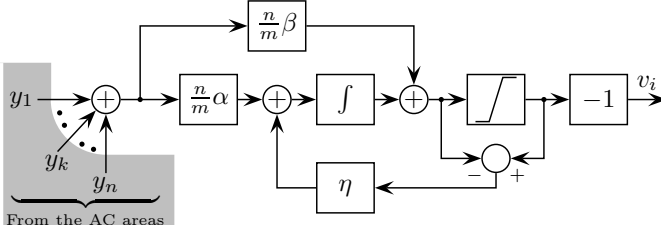
Figure 2. Control strategy applied to the i-th WPP ($i = 1, \ldots, m$)

Figure 3. Control strategy applied to the i-th AC area ($i = 1, \ldots, n$)

The proposed control scheme consists of two levels. The first level is the DC voltage control, which is responsible for ensuring the power transmission under normal conditions. This is a master-slave scheme with the n-the AC area acting as the master and the rest of AC areas and WPPs as slaves. The voltage control at n-th AC area ensures that $V_{dc,n} = V_{dc,\text{ref}}$. The second level control regulates the frequency of the AC areas and ensures the proper contribution of the WPPs. This level imposes the DC power injected and extracted by each station in order to compensate the frequency deviations. The aim of this second level is to provide inertial and primary frequency control for the AC areas.

The second level control at the i-th WPP imposes the power injected into the multi-terminal grid by the WPPs and is implemented as

$$P_{w,i} - \bar{P}_{w,i} = v_i = \begin{cases} v_{\min,i}, & \hat{v}_i < v_{\min,i}, \\ \hat{v}_i, & v_{\min,i} \le \hat{v}_i < v_{\max,i}, \\ v_{\max,i}, & \hat{v}_i \ge v_{\max,i}, \end{cases} \quad (5)$$

for all $i = 1, \ldots, m$, with $\bar{P}_{w,i}$ the nominal power injected by the i-th WPP, $v_{\min,i}$ and $v_{\max,i}$ are the lower and upper power reserve limits, respectively,

$$\hat{v}_i = -\frac{n}{m} \sum_{k=1}^{n} \left(\alpha \int y_k dt + \beta y_k \right), \quad (6)$$

and α and β are parameters to be tuned. The signal v_i is the active power contributed by the i-th WPP with respect to the nominal operating point. The control strategy applied at each WPP is sketched in Fig. 2. As the power reserve in the WPP is limited and depends on the wind speed conditions, during some time some or all of the v_i could reach the saturation limits. Therefore, the control strategy also includes a back-calculation algorithm to mitigate wind-up effects. The symbol η in Fig. 2 is a positive gain governing the anti-windup compensation, a typical value is $\eta = 1/\sqrt{\alpha\beta}$ [24].

The second level control at the i-th AC area power converter aims at regulating the power extracted from the DC grid and is given by

$$u_i = \underbrace{\sum_{\substack{k=1 \\ k \neq i}}^{n} \left(\alpha \int (y_i - y_k) dt + \beta (y_i - y_k) \right)}_{\text{consensus algorithm}} - \underbrace{\frac{1}{n} \sum_{k=1}^{m} v_k}_{\substack{\text{WPP} \\ \text{contribution}}}, \quad (7)$$

for all $i = 1, \ldots, n$. The first term in (7) is a consensus algorithm. The second terms represent the power injected by the WPPs into the MT-HVDC grid. This control scheme is shown in Fig. 3.
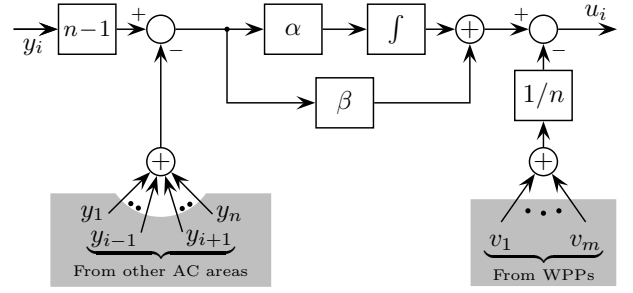
The control law (5) and (7) satisfies

$$\underbrace{\sum_{i=1}^{n} u_i}_{\substack{\text{AC area} \\ \text{contribution}}} + \underbrace{\sum_{i=1}^{m} v_i}_{\substack{\text{WPP} \\ \text{contribution}}} = 0. \quad (8)$$

That is, the total power incoming and outgoing from the multi-terminal grid remains unchanged. Notice that as the low level control ensures that $V_{dc,n} = V_{dc,\text{ref}}$, the control law (7) is not explicitly implemented in the n-th AC area. Nevertheless, the power u_n obeys (7) since the total power change must be zero.

The expressions (5) and (7) form a distributed control law that adapts to the wind power conditions to provide primary frequency control and is capable of restoring the frequency if sufficient wind power is available. The strategy uses communications (*e.g.* fiber optic in the cables) in order that the stations share a set of signals. Each AC area sends its frequency and each WPP sends its power contribution to the rest of the stations. If the change in the power demand is small enough to be compensated with the total contribution of the WPPs, the proposed control scheme is capable of restoring the frequency in all AC areas to the nominal value $f_{\text{nom},i}$. In this case, $\hat{v}_i = \hat{v}$ and $v_{i,\min} < \hat{v} < v_{i,\max}$ for all $i = 1, \ldots, m$ (see Appendices for more details). Therefore, the last term in (7) reduces to $(m/n)\hat{v}$ leading to

$$u_i = \alpha \int y_i dt + \beta y_i, \quad i = 1, \ldots, n.$$

This is a local PI controller driving the frequency at each AC area towards its nominal value, *i.e.*

$$y_i \to \hat{y}^e = 0, \quad \forall\, i = 1, \ldots, n.$$

In case the power demand is too high or too low, WPPs deliver the maximum or the minimum power available and the rest is provided from the other AC areas until reaching a consensus frequency by sharing their power reserves. In cases in which all WPPs are delivering $v_{\max,i}$ or $v_{\min,i}$, expression (7) reduces to a typical consensus algorithm. In this case (see Appendix A for details), the consensus algorithm ensures that the frequency deviations in all AC areas converge to

$$y_i \to \hat{y}^e = -\left(\sum_{i=1}^{n} d_i - \sum_{i=1}^{m} v_{i,\text{sat}} \right) \Big/ \sum_{i=1}^{n} r_i, \quad (9)$$

for $i = 1, \ldots, n$, where $r_i = a_{1i}/a_{2i} + a_{4i}/a_{3i}$ and $v_{i,\text{sat}}$ denotes $v_{\min,i}$ or $v_{\max,i}$. It can be noted that final frequency

deviation still depends on the WPP contribution and the deviation will be smaller than in the case without WPP support.

The control strategy (5) and (7) can be interpreted as an extension of those proposed in [15], [16]. Equation (5) and the last term in (7) allow using the converters at WPPs (stations in which it is not necessary to control the frequency) to reduce frequency deviations in the AC areas and even restoring the frequency when sufficient power reserves are available. The proposed control strategy can also be seen as an extension of the voltage-frequency droop and weighted frequency scheme (WFS) introduced in [17], [21], respectively. These schemes are also consensus algorithm as in (7) with $\alpha = 0$. These schemes stabilize the frequency, but the frequencies on the AC areas converge to different values depending on the power sharing. This makes more difficult to predict the frequency in the AC areas after changes in the power demands.

The proposed control strategy requires to tune only two parameters α and β. Using similar arguments to those presented in [16], it is possible to prove that the closed-loop system is stable for all positive values of α and β. However, this does not guarantee a fast convergence to the new frequency after a power demand disturbance. Here, we propose a tuning procedure based on robust control arguments to ensure stability and a proper response in all power reserve conditions [25].

For control design purposes, the closed-loop system can be cast as in Fig. 4, where the plant and the controller are

Figure 4. Closed-loop system representation for control design purposes

$$G(s) = \begin{bmatrix} G_1(s) & \cdots & 0 \\ \vdots & \ddots & \vdots \\ 0 & \cdots & G_n(s) \end{bmatrix},$$

with $G_i(s) = C_i(sI - A_i)^{-1}B_i$,

$$A_i = \begin{bmatrix} -a_{1,i} & a_{2,i} \\ -a_{3,i} & -a_{4,i} \end{bmatrix}, \quad B = \begin{bmatrix} -a_{2,i} \\ 0 \end{bmatrix}, \quad C = \begin{bmatrix} 1 & 0 \end{bmatrix},$$

the controller is

$$K(s) = \begin{bmatrix} K_1(s) & \cdots & 0 \\ \vdots & \ddots & \vdots \\ 0 & \cdots & K_n(s) \end{bmatrix},$$

with $K_i(s) = \alpha/s + \beta$ and Δ a constant matrix gain. As $G(s)$ and $K(s)$ are decoupled systems, the transfer function $T_{zy}(s)$ from y to z is also a decoupled plant. Therefore, the parameters α and β can be tuned with classical PI rules with the subsequent verification of the following condition

$$\|T_{zy,i}(s)\|_\infty = \max_\omega \left| \frac{G_i(\jmath\omega)K_i(\jmath\omega)}{1 + G_i(\jmath\omega)K_i(\jmath\omega)} \right| \le \frac{1}{n}, \quad (10)$$

for all $i = 1, \ldots, n$ (see Appendix B for details).

Alternatively, the controller parameters α and β can be tuned using $\mathcal{H}_\infty$ optimal control tools in order to balance the frequency regulation and the power profiles demanded to the WPPs [25]. To this end, condition (20) can be complemented with additional constraints on the transfer functions from d to y and u in order to ensure a suitable convergence to the nominal frequency with reasonable control action. This implies to add the condition

$$\left\| \begin{matrix} W_e(s)T_{dy}(s) \\ W_u(s)T_{du}(s) \end{matrix} \right\|_\infty \le \gamma, \quad (11)$$
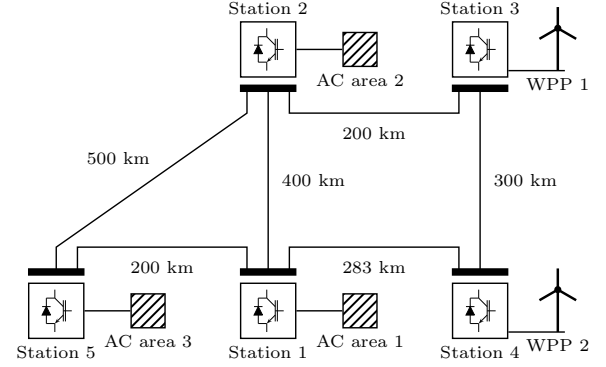

Figure 5. Multi-terminal HVDC network corresponding to the case study

with γ a positive scalar, $W_e(s)$ and $W_u(s)$ weighting functions to shape the frequency response of the desire transfer functions. With this setup, the parameters α and β can be obtained by solving an optimization problem like those presented in [26], [27].

IV. CASE STUDY

The proposed control scheme is illustrated by simulation in a well-accepted multi-terminal network [28] adapted for frequency control studies. The simulations were carried out in MATLAB/SimPowerSystems. The power system under study (sketched in Fig. 5) connects two WPPs with three AC areas. As indicated in Section III, the voltage control implemented in the MT-HVDC grid is based on a master-slave scheme. In this case, the converter in AC area 3 is defined as the master station responsible for regulating the DC voltage at the other terminals. The parameters considered for the dynamics of each synchronous AC grid and the line resistances of the DC network are listed in Table I. The wind farms are modelled as aggregated wind turbines. WPP 1 consists of eight 5 MW-turbines and WPP 2 of six 5 MW-turbines. The wind turbine models correspond to the NREL benchmark turbine with the power control like those in [29]. This control allows tracking a power reference in order to implement the power reserve by pitching [30]. The active power generation in AC areas 1, 2 and 3 are 40 MW, 60 MW and 150 MW, respectively. The nominal DC voltage is $V_{dc,5} = V_{dc,\mathrm{ref}} = 400$ kV.

The control parameters were tuned according to the procedure presented in the previous section. The weighting functions in (11) were selected as

$$W_e(s) = 20\left(\frac{s/20 + 1}{s/0.2 + 1}\right)^2, \quad W_u(s) = 5\frac{s+1}{s/100 + 1}.$$

Table I
PARAMETERS FOR THE MULTI-TERMINAL HVDC NETWORK EXAMPLE

AC area	1	2	3
J (kgm^2)	4863	6078	6485
D_g (Ws^2)	95.00	140.00	146.40
τ_m (s)	2.00	2.50	2.50
σ	0.04	0.06	0.04
P_{nom} (MW)	40	60	150
$f_{\text{nom},i} = 50$ Hz, $D_{l,i} = 0.1$ s, $\bar{P}_{m,i} = P_{\text{nom},i}, \forall i = 1, 2, 3$			
Line resistances	$R_{12} = 7.60\,\Omega$	$R_{14} = 5,37\,\Omega$	$R_{15} = 3.80\,\Omega$
	$R_{23} = 3.80\,\Omega$	$R_{25} = 9.50\,\Omega$	$R_{34} = 5.70\,\Omega$

The weight W_e penalizes the frequency errors and W_u the control actuation in order to obtain a controller ensuring a fast convergence to the nominal frequency with a reasonable control action [25]. After solving the optimization problem, the parameters for the proposed frequency control algorithm resulted

$$\alpha = 20.76 \text{ MW}, \qquad \beta = 8.16 \text{ MWs}.$$

A. Power demand changes on the AC synchronous areas

The first scenario aims to evaluate the system responses under changes in the power demand in the AC area 1 and 2. It is worth recalling that all AC grids are independent, and only electrical linked through the MT-HVDC network. Initially, the WPPs are injecting a total of 63 MW ($\bar{P}_{w,1} = 36$ MW and $\bar{P}_{w,1} = 27$ MW), which corresponds to a power reserve of 10% when the wind turbines operate above rated wind speed (region 3). In this scenario, the wind speed was set at 13 m/s. The demands at the AC areas are $P_{l,1} = 58$ MW, $P_{l,2} = 75$ MW and $P_{l,5} = 180$ MW. The power demand in the AC area 2 increases in 7% (5.25 MW) at $t = t_1$ and in the AC area 1 an increase of 6% (3.48 MW) occurs at $t = t_2$ as shown in Fig. 6b. The effects of these disturbances on the frequencies of the AC synchronous areas without the proposed control scheme are shown in Fig. 6a. It can be observed that in both cases the NADIR frequency is going below 49.80 Hz (a value not admissible according to the grid codes) and also that the new steady-state frequency is quite low. Therefore, a frequency control is needed to at least reduce the deviation from the rated value 50 Hz.

The system response with the proposed control strategy is shown in Fig. 7. The evolution of the frequency at each AC area can be seen in Fig. 7a and both injected and extracted powers (with respect to the steady-state values) by each converter station from the MT-HVDC network is plotted in Fig. 7b. To compensate the increase in the power demand, the control imposes an equal contribution to both WPPs. In the first stage ($t_1 \leq t \leq t_2$), the WPPs are capable of injecting the power needed to restore the frequency in AC area 2, and the frequencies in the other areas remain almost unaffected. When an additional power demand increase in the AC area 3 occurs (at $t = t_2$), WPP 2 reaches the reserve limit. This forces to increase the contribution of WPP 1, which also exhausts its reserve. In this stage, the total wind power reserve are not sufficient to restore the frequency to the nominal value. As a
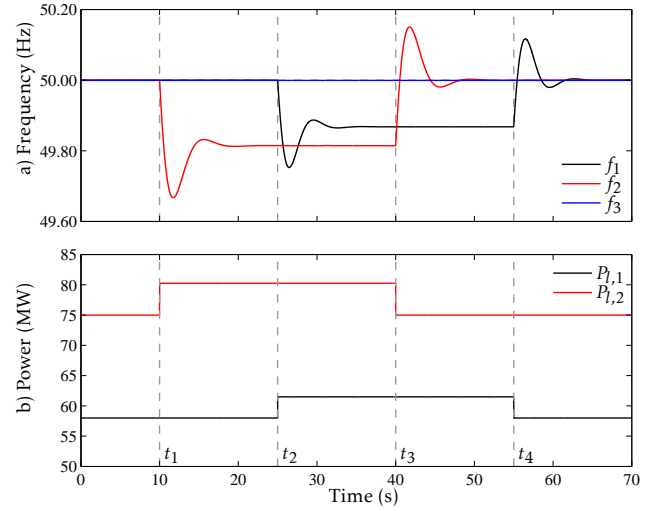

Figure 6. Frequency evolution under different changes in the power demand in AC area 2 and 3 without frequency control and corresponding power demand disturbances
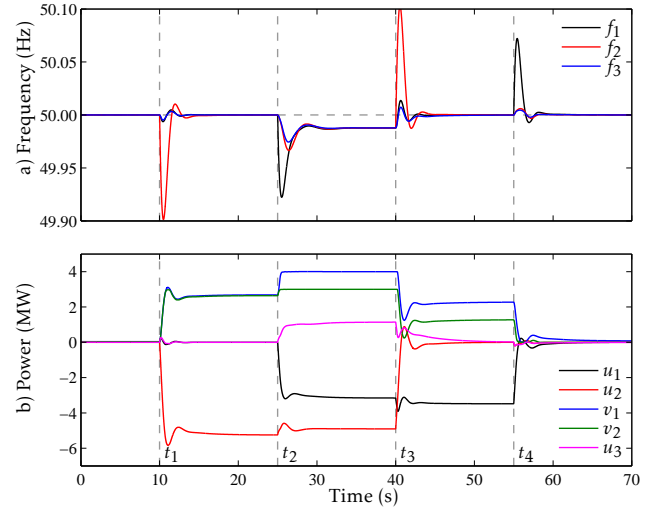

Figure 7. Closed-loop system response under different changes in the power demand in AC area 1 and 2 with the proposed frequency control scheme

consequence, the other AC areas must contribute to reach a consensus frequency. According to (9), this frequency is given by

$$f^e = 50 \text{ Hz} - \underbrace{(3.48 \text{ MW} + 5.25 \text{ MW})}_{d_1 + d_2} -$$
$$- \underbrace{(4 \text{ MW} + 3 \text{ MW})}_{v_1 + v_2}) / \underbrace{(147.05 \text{ MW/Hz})}_{r_1 + r_2 + r_3} = 49.99 \text{ Hz}.$$

It must be noted that although the wind power is not sufficient to restore the frequency to the rated value, the contribution of the WPPs helps to mitigate the frequency deviation in all areas. After 30 s ($t = t_3$) from the beginning of the first power disturbance, the secondary frequency control in area 2 compensates the power demand increasing the generation. As a result, the wind power reserve is now sufficient to restore

the frequency and recovers part of the power reserve. When the secondary frequency control in area 1 also increases the generation, all stations return to the initial states and the WPPs fully recover the power reserve of 10%.

B. Drop in the wind power

The second scenario analyzes the behavior under a wind power drop as a consequence of a reduction in the wind speed. Fig. 8 shows the closed-loop system response under an increase in the power demand of 5% in AC area 2 and a wind power drop. At $t = t_1$, the power demand $P_{l,2}$ increases in 3.75 MW. As shown in the previous case, since the power reserve is sufficient, the control succeeds in conducting the frequency to the nominal value without significantly affecting the frequencies in the other AC areas. The frequencies and power deviations are shown in Fig. 8a and b. Later, at $t = t_2$, the wind speed in wind farm 2 decreases and the power delivered by WPP 2 starts to decrease at $t = t_3$ as shown in Fig. 8b and c. In this case, the control algorithm tries to compensate this power reduction by increasing the contribution of WPP 1, which in turn exhausts its power reserve. As a result, the rest of the AC areas must contribute to stop the frequency drop as can be seen in Fig. 8. Under this circumstance, the consensus frequency is 49.97 Hz according to (9). At $t = t_4$, the power demand in AC area 2 return to the initial values but this is not sufficient to restore the frequency at the nominal value. Notice that under this circumstance, the propose control strategy also attain the most reasonable frequency regulation. This scenario shows that the proposed control scheme allows wind farms to provide frequency support and AC area to share power in order to mitigate frequency drop under low wind power conditions.

C. Communications faults

The last scenario evaluates the robustness of the proposed scheme against faults in the communications. Fig. 9 shows the closed-loop response under the power demand changes analyzed in Fig. 7 when AC area 2 are not able to send the frequency measure to other stations. This is a worst-case scenario in which the power disturbance occurs in the station with communications problems. Nevertheless, it can be observed that the proposed strategy is robust as the response is slightly affected compared with the results in Fig. 7. With sufficient wind power reserve, the system is slower but is still capable of restoring the frequency. In this situation, the rest of the stations do not have direct information about the frequency deviations in AC area 2. The stations react under the frequency deviation observed in AC area 1 caused by the low level control seeking the power balance. As a result, the frequency regulation is slower than in faultless conditions. The frequency regulation is more affected under high power demand conditions ($t_2 \leq t \leq t_3$). In this circumstance, the consensus algorithm cannot force the converge to a common frequency although the frequency is still stabilized at a value close to nominal.

V. CONCLUSIONS

The paper presents a primary frequency control scheme in order that WPPs connected through MT-HVDC are able to
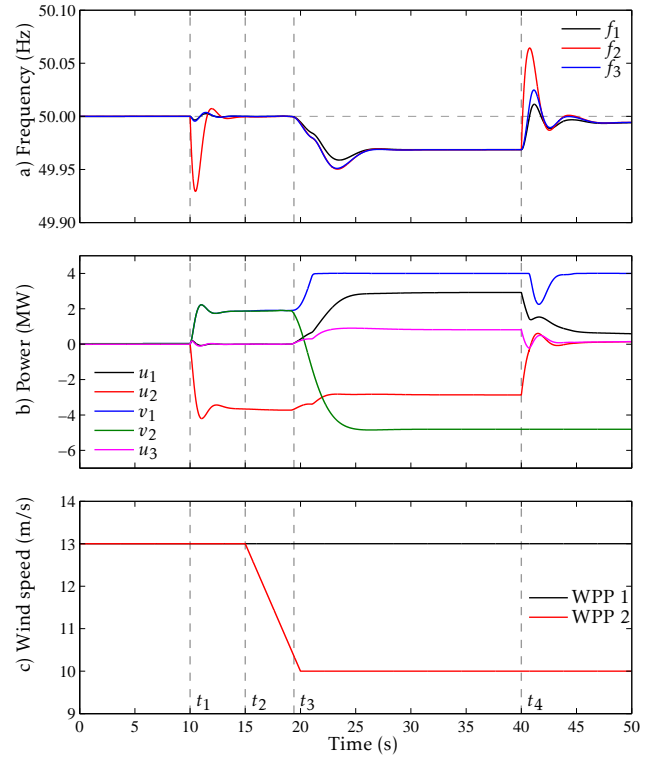

Figure 8. Closed-loop system response under an increase on the power demand in AC area 2 and drop in the wind power
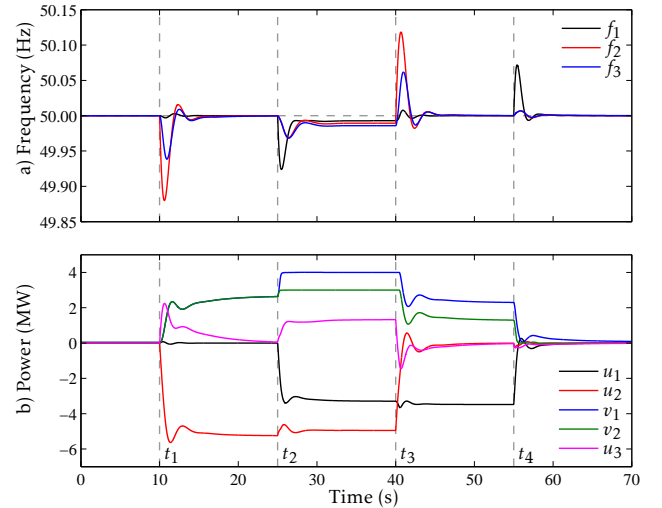
Figure 9. Closed-loop system response under different changes in the power demand in AC area 1 and 2 with the proposed frequency control with not communications from area 2

contribute to the frequency support of the land AC networks. The proposed control scheme is distributed (without a main supervisor) to take into account that AC areas and WPPs can be operated by different system players. The scheme also considers the limited power reserve in WPPs and adapts itself to achieve the most suitable frequency regulation according to the available power reserve in the WPPs. Under small power demand changes, the control is capable of restoring

the frequency in the AC areas to the rated value. In case of large power demands, the control strategy permits all stations to share their power reserves in order that the frequency in all AC areas converges to a value close to nominal frequency. The proposed control scheme was validated by transient simulations in a well-accepted 5-bus MT-HVDC grid with two WPPs under representative scenarios showing the capability of the scheme to achieve a proper primary frequency control even under severe communications faults.

APPENDIX

Defining L as the Laplacian matrix of the communication graph among the different AC areas and WPPs with elements

$$[L]_{ij} = \begin{cases} -1 & \text{for } i \neq j, \\ n-1 & \text{for } i = j, \end{cases}$$

the matrix H_l of dimension $1 \times m$ and elements

$$[H_l]_i = \begin{cases} 0 & \text{if the } i\text{-th WPP is saturated}, \\ 1 & \text{otherwise}, \end{cases}$$

and $\mathbf{1}_{n \times 1}$ is an all-ones matrix of dimensions $n \times 1$, the control laws (5) and (7) result

$$\mathbf{u} = \alpha \int L\mathbf{y} dt + \beta L\mathbf{y} - \frac{1}{n}\mathbf{1}_{n \times 1}(H_l\mathbf{v} + \bar{H}_l\mathbf{v}_{\text{sat}}), \quad (12)$$

$$\hat{v}_i = -\frac{n}{m}\left(\alpha \int \mathbf{1}_{1 \times n}\mathbf{y} dt + \beta \mathbf{1}_{1 \times n}\mathbf{y}\right), \quad (13)$$

with $\bar{H} + H = \mathbf{1}_{n \times 1}$,

$$\mathbf{y} = [y_1, \ldots, y_n]^T, \qquad \mathbf{u} = [u_1, \ldots, u_n]^T,$$
$$\mathbf{v} = [v_1, \ldots, v_m]^T, \qquad \mathbf{v}_{\text{sat}} = [v_{1,\text{sat}}, \ldots, v_{m,\text{sat}}]^T.$$

The subscript l denotes one of the 2^m configurations corresponding to the saturation state of each WPP and the subscript sat denotes the lower or upper power limits.

If all integral parts in (6) start from equal initial conditions, $\hat{v}_i$ can be assumed equal to a common value $\hat{v}$. Therefore, the control law (12) reduces to

$$\mathbf{u} = \alpha \int F_l\mathbf{y} dt + \beta F_l\mathbf{y} - \frac{1}{n}\mathbf{1}_{n \times 1}\bar{H}_l\mathbf{v}_{\text{sat}}, \quad (14)$$

with $F_l = L + \frac{q_l}{m}\mathbf{1}_{n \times n}$, $l = 1, \ldots, 2^m$, and q_l the number of WPPs that have not reached the power reserve limits. Then, the closed-loop system is given by

$$\frac{d}{dt}\mathbf{z} = \underbrace{\begin{bmatrix} -A_1 & A_2 & -A_2 \\ -A_3 & -A_4 & 0 \\ A_{5,l} & \beta F_l A_2 & -\beta F_l A_2 \end{bmatrix}}_{A_{cl,l}}\mathbf{z} - \begin{bmatrix} A_2 \\ 0 \\ \beta F_l A_2 \end{bmatrix}\mathbf{d}, \quad (15)$$

where $A_{5,l} = F_l(\alpha I - \beta A_1)$, I is the identity matrix, $\mathbf{x}^T = [x_1, \ldots, x_n]$, $\mathbf{d}^T = [d_1, \ldots, d_n]$, $\mathbf{z}^T = [\mathbf{y}^T \ \mathbf{x}^T \ \mathbf{u}^T]$, and

$$A_j = \begin{bmatrix} a_{j,1} & \cdots & 0 \\ \vdots & \ddots & \vdots \\ 0 & \cdots & a_{j,n} \end{bmatrix}, \qquad j = 1, \ldots, 4.$$

A. Equilibrium points

The equilibrium point is obtained by replacing the left term of (15) by the zero vector and solving the resulting algebraic equation. The frequencies at the equilibrium are given by

$$F_l\mathbf{y}^e = 0. \quad (16)$$

This equilibrium point depends on the power reserve in each WPP. There are three possible cases:

a) Case 1: All WPPs having sufficient power reserves: This implies that $v_{i,\min} < \hat{v} < v_{i,\max}$ for all $i = 1, \ldots, m$ and

$$F_1 = nI. \quad (17)$$

In this circumstance, the only solution for (16) is $\mathbf{y}^e = 0$. Therefore, the frequency at each AC area will converge to the nominal values $f_{\text{nom},i}$. In this case, the dynamic equations of each area are decoupled and the control parameters α and β can be tuned using any rules for PI controllers.

b) Case 2: Some of WPPs without sufficient power reserve: Assuming that only $q_l < m$ WPPs have not reached the power reserve limits, so that the total wind power contribution is sufficient to restore the frequency in the AC areas, the matrix F_l results

$$F_l = \begin{bmatrix} n + \frac{q_l}{m} - 1 & \frac{q_l}{m} - 1 & \cdots & \frac{q_l}{m} - 1 \\ \frac{q_l}{m} - 1 & n + \frac{q_l}{m} - 1 & \vdots & \frac{q_l}{m} - 1 \\ \vdots & \vdots & \ddots & \vdots \\ \frac{q_l}{m} - 1 & \cdots & \cdots & n + \frac{q_l}{m} - 1 \end{bmatrix}. \quad (18)$$

Clearly, the rows in F_l are linear independent and thus the matrix F_l is nonsingular. Therefore, the only solution for (16) is $\mathbf{y}^e = 0$. This demonstrates that, with sufficient power reserve in the WPPs, the proposed scheme can restore the frequency of the AC areas to the nominal values.

c) Case 3: All WPPs without sufficient power reserve: This corresponds to the case in which the total WPP contribution is not sufficient to restore the frequency in the AC areas. All signals v_i are reached the reserve limits, $q_l = 0$ and the matrix F_l reduces to L. The control law (5) reduces to a consensus algorithm that allows all AC areas to help in the frequency stabilization in a common value. The matrix L has one eigenvalue in 0 with eigenvector $\mathbf{1}_{1 \times n}$ [31], that is, the equilibrium point is given by

$$\mathbf{y}^e = \mathbf{1}_{n \times 1}\hat{y}^e.$$

The value $\hat{y}^e$ can be computed from equaling (15) to zero, then

$$r_i y^e = u_i + v_{i,\text{sat}},$$

with $r_i = a_{1i}/a_{2i} + a_{4i}/a_{3i}$. Equation (9) is obtained by adding from $i = 1$ to n and using (8).

B. Stability and control tuning

Here, we propose a tuning procedure based on robust control arguments to ensure stability and a proper response in all power reserve conditions [25].

From the Small Gain Theorem [25], the closed-loop system in (15) is stable under any saturation configurations if the condition

$$\|T_{zy}(s)\|_\infty \le (\|\Delta\|_2)^{-1} = \frac{m}{n(m - q_l)}, \qquad (19)$$

with $\Delta = \frac{q_l - m}{m} \mathbf{1}_{n \times n}$, is satisfied, *i.e.*, the infinity norm of the transfer function from z to y is lower than $m/n(m - q_l)$. The most restrictive scenario corresponds to $q_l = 0$ leading to

$$\|T_{zy}(s)\|_\infty \le 1/n. \qquad (20)$$

As $G(s)$ and $K(s)$ are decoupled systems, the transfer function $T_{zy}(s)$ is also a decoupled plant. Therefore, condition (20) implies that maximum amplitude of the frequency response of the individual transfer functions $T_{zy,i}(s)$ must be lower than $1/n$, which is equivalent to condition (10).

REFERENCES

[1] A. Arapogianni, J. Moccia, and J. Wilkes, "The European offshore wind industry - key trends and statistics 2012," European Wind Energy Association, Tech. Rep., 2013.

[2] S. Gordon, "SuperGrid to the rescue," *IET Power Eng.*, vol. 20, no. 5, pp. 30–33, 2006.

[3] D. Van Hertem and M. Ghandhari, "Multi-terminal VSC HVDC for the European supergrid: Obstacles," *Renewable Sustainable Energy Rev.*, vol. 14, pp. 3156–3163, 2010.

[4] J. Liang, T. Jing, O. Gomis-Bellmunt, J. Ekanayake, and N. Jenkins, "Operation and Control of Multiterminal HVDC Transmission for Offshore Wind Farms," *IEEE Trans. Power Delivery*, vol. 26, no. 4, pp. 2596–2604, 2011.

[5] ENTSO-E, "Network code for requirements for grid connection applicable to all generator," 2013.

[6] ——, "Draft network code on high voltage direct current connection and DC–connected power park modules," Apr. 2014.

[7] "P.O. 12.2: Installations connected to transmission networks: minimum requirements for design, equipment, operation and commissioning (in spanish)," in *Official State Gazette (BOE)*, no. 51. Ministry of Industry, Energy and Tourism, Spain, March 2005, pp. 7416–7423.

[8] F. Díaz-González, M. Hau, A. Sumper, and O. Gomis-Bellmunt, "Participation of wind power plants in system frequency control: Review of grid code requirements and control methods," *Renewable Sustainable Energy Rev.*, vol. 34, pp. 551–564, 2014.

[9] P. M. Anderson and A. A. Fouad, *Power System Control and Stability*, 2nd ed. New York, USA: John Wiley & Sons Inc, 2002.

[10] O. Anaya-Lara, N. Jenkins, J. Ekanayake, P. Cartwright, and M. Hughes, *Wind Energy Generation: Modelling and Control*. Chicester, UK: John Wiley & Sons, 2009.

[11] J. Morren, S. de Haan, W. Kling, and J. Ferreira, "Wind turbines emulating inertia and supporting primary frequency control," *IEEE Trans. Power Syst.*, vol. 21, no. 1, pp. 433–434, 2006.

[12] R. G. de Almeida and J. A. Pecas Lopes, "Participation of doubly fed induction wind generators in system frequency regulation," *IEEE Trans. Power Syst.*, vol. 22, no. 3, pp. 944–950, 2007.

[13] N. Ullah, T. Thiringer, and D. Karlsson, "Temporary primary frequency control support by variable speed wind turbines – potential and applications," *IEEE Trans. Power Syst.*, vol. 23, no. 2, pp. 601–612, 2008.

[14] J. Aho, A. Buckspan, and J. H. Laks, "A tutorial of wind turbine control for supporting grid frequency through active power control," in *Proc. of the American Control Conference*, 2012, pp. 3120–3131.

[15] J. Dai, Y. Phulpin, A. Sarlette, and D. Ernst, "Coordinated primary frequency control among non-synchronous systems connected by a multi-terminal high-voltage direct current grid," *IET Gener. Transm. Distrib.*, vol. 6, no. 2, p. 99, 2012.

[16] A. Sarlette, J. Dai, Y. Phulpin, and D. Ernst, "Cooperative frequency control with a multi-terminal high-voltage DC network," *Automatica*, vol. 48, no. 12, pp. 3128–3134, Dec. 2012.

[17] N. Chaudhuri, R. Majumder, and B. Chaudhuri, "System frequency support through multi-terminal DC (MTDC) grids," *IEEE Trans. Power Syst.*, vol. 28, no. 1, pp. 347–356, 2013.

[18] M. Andreasson, R. Wiget, D. V. Dimarogonas, K. H. Johansson, and G. Andersson, "Distributed primary frequency control through multi-terminal HVDC transmission systems," in *Proc. of the American Control Conference*, Chicago, USA, 2015.

[19] A. M. Bucurenciu, "Primary frequency response by MTDC offshore grids," Master's thesis, Delft University of Technology, 2012.

[20] B. Silva, C. Moreira, L. Seca, Y. Phulpin, and J. Peças-Lopez, "Provision of inertial and primary frequency control services using offshore multi-terminal HVDC networks," *IEEE Trans. Sustain. Energy*, vol. 3, no. 4, pp. 800–808, 2012.

[21] I. Martinez Sanz, B. Chaudhuri, and G. Strbac, "Inertial response from offshore wind farms connected through DC grids," *IEEE Trans. Power Syst.*, vol. 30, no. 3, pp. 1518–1527, 2015.

[22] P. Kundur, *Power System Stability and Control*. New York, USA: McGraw-Hill, 1994.

[23] P. Sorensen, A. D. Hansen, F. Iov, F. Blaabjerg, and M. H. Donovan, "Wind farm models and control strategies," RISO, Tech. Rep., 2005.

[24] K. Åström and T. Hägglund, *PID Controllers*, ser. Setting the standard for automation. Research Triangle Park; USA: ISA, 1995.

[25] K. Zhou, J. C. Doyle, and K. Glover, *Robust and Optimal Control*. Upper Saddle River, USA: Prentice Hall, 1995.

[26] S. Gumussoy, M. Millstone, and M. L. Overton, "H∞ strong stabilization via HIFOO, a package for fixed-order controller design," in *Proc. of the 47th Conference on Decision and Control*, 2008, pp. 4135–4140.

[27] P. Apkarian, "Tuning controllers against multiple design requirements," in *Proc. of the American Control Conference*, 2012, pp. 3888–3893.

[28] "Guide for the development of models for HVDC converters in a HVDC grid," Working Group B4.57, Cigré, Tech. Rep., 2015.

[29] J. Jonkman, S. Butterfield, W. Musial, and G. Scott, "Definition of a 5-MW reference wind turbine for offshore system development," NREL, Golden, Colorado, USA, Tech. Rep. NREL/TP-500-38060, 2009.

[30] T. Knudsen, T. Bak, and M. Svenstrup, "Survey of wind farm control-power and fatigue optimization," *Wind Energy*, vol. 18, no. 8, pp. 1333–1351, 2015.

[31] R. Olfati-Saber, J. A. Fax, and R. M. Murray, "Consensus and cooperation in networked multi-agent systems," *Proc. IEEE*, vol. 95, no. 1, pp. 215–233, 2007.

F.D. Bianchi received the B.S. and Ph.D. degrees in electronic engineering from the National University of La Plata (UNLP), Argentina, in 1999 and in 2005, respectively. From 1999 to 2006, he was a Ph.D. student and a Postdoctoral Fellow at the LEICI (UNLP, La Plata, Argentina). From 2006 to 2010, he was a Postdoctoral Researcher at the Technical University of Catalonia (UPC), Barcelona, Spain. In 2010, he joined the Power Electronics and Electric Power Grids Group, Catalonia Institute for Energy Research (IREC), Barcelona, as a Scientific Researcher. His main research interests include robust control and linear parameter-varying systems and their applications to the control of renewable energy conversion systems.

J.L. Domínguez-García (S'11-M'13) received the B.S.and M.S. degrees in industrial engineering from the School of Industrial Engineering of Barcelona, UPC, Barcelona, Spain. in 2009. He developed his master's thesis in Oulun Yliopisto, Oulu, Finland. In 2013 he received the Ph.D. degree in electrical engineering from UPC with a qualification of Excellent "Cum Laude". He received the Outstanding PhD Thesis award from UPC in 2015. Since 2010 he is researcher in the Catalonia Institute for Energy Research (IREC). He was an Academic Visitor of the Institute of Energy, Cardiff University, Wales, UK, in 2011. His research interest are modelling and control of electrical machines and power converters, renewable energy integration in power systems, power system dynamics, and linear system theory.